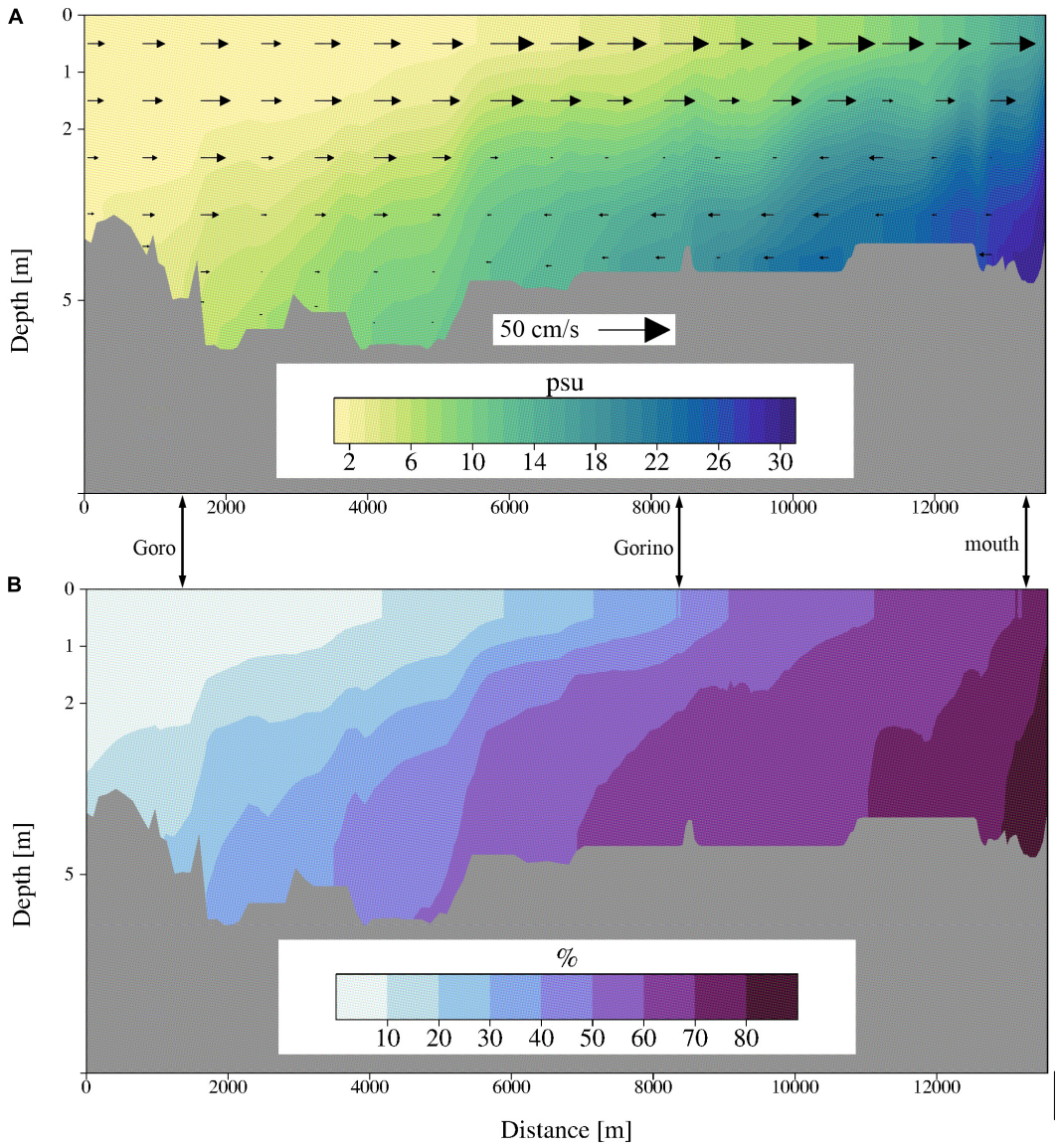

FIGURE 9 | (A) Period July–October 2018: average salinity along the axis of the Po di Goro branch and superimposed average current. **(B)** Percentage of salinity values higher than 2 PSU along the axis of the Po di Goro branch during the 2018 year. Distances in m are from upstream to the river mouth.

changes also the mixing in the Lagoon as recently explained for estuaries in Burchard (2020).

THE GOLFEM MODEL FOR THE "WHAT IF" SCENARIOS

The calibration and validation of the Goro Lagoon numerical model will facilitate "What if" scenarios to be carried out for the sustainable management of the site. The lagoon is a key area for clam farming in Italy. The economic activities are coordinated by a consortium of around 1400 local producers who, together with the local government authorities, helped to co-design the "What if" numerical experiments.

The ecosystem health and productivity levels of the lagoon are connected to the area's morphology and dynamics, the hydrodynamic regime, the freshwater inputs, water salinity, and the specific ecosystem of the area. All these aspects interact to produce suitable conditions for the biological productivity of the lagoon. The question to be addressed by the "What if" scenarios is how to modify some of these key factors for the future sustainable exploitation of resources. To do this, a numerical model is needed that encompasses most of the interacting processes in the Lagoon, so that all the feedback can be considered. With a purely hydrodynamic model, like the one presented in this paper, we can address factors related to the morphology, the hydrodynamics, freshwater inputs, and the water salinity. In the future, if the complexity of the model is increased with sediment transport and

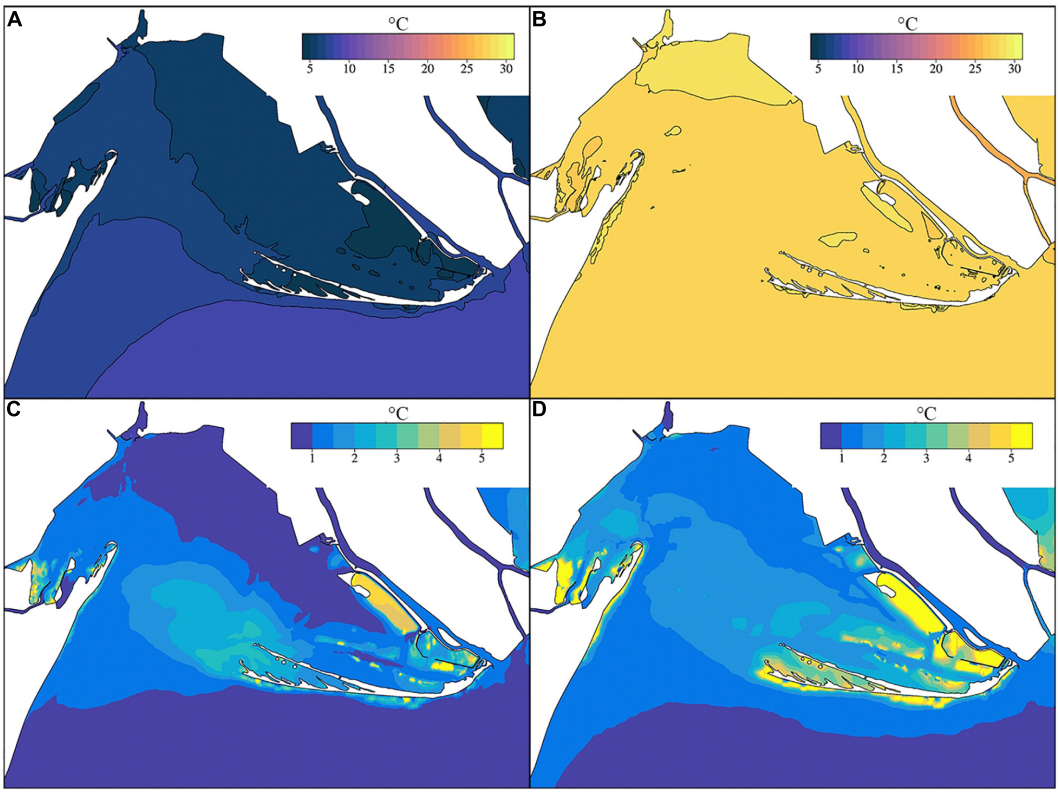

FIGURE 10 | Average temperature of the water column in February **(A)**, August **(B)** and average daily range (daily maximum – daily minimum) in February **(C)**, August **(D)** 2018.

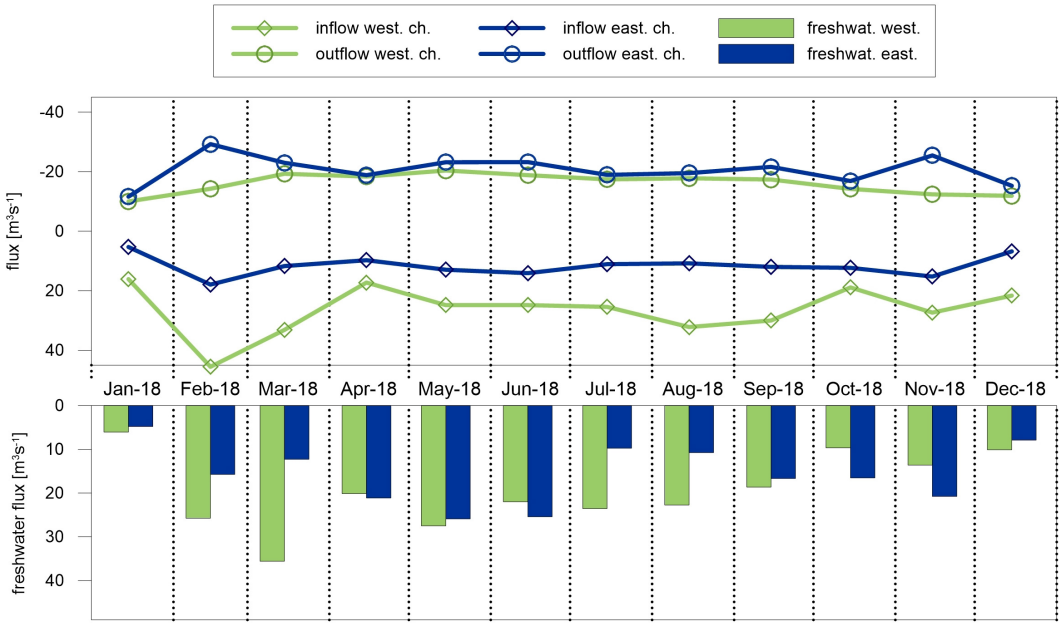

FIGURE 11 | Average volume fluxes in the inlet channels, distinguished by inflow positive (in the deeper layers) and negative outflow in the surface layer. The average freshwater inputs in the lagoon are considered positive. The western freshwater is the sum of the Po of Volano and the pumping stations Giralda (G), Romanina (R), and Bonello (B) (**Figure 1**), The eastern freshwater is the sum of the volume fluxes at the Manufatto gate and Gorino lock.

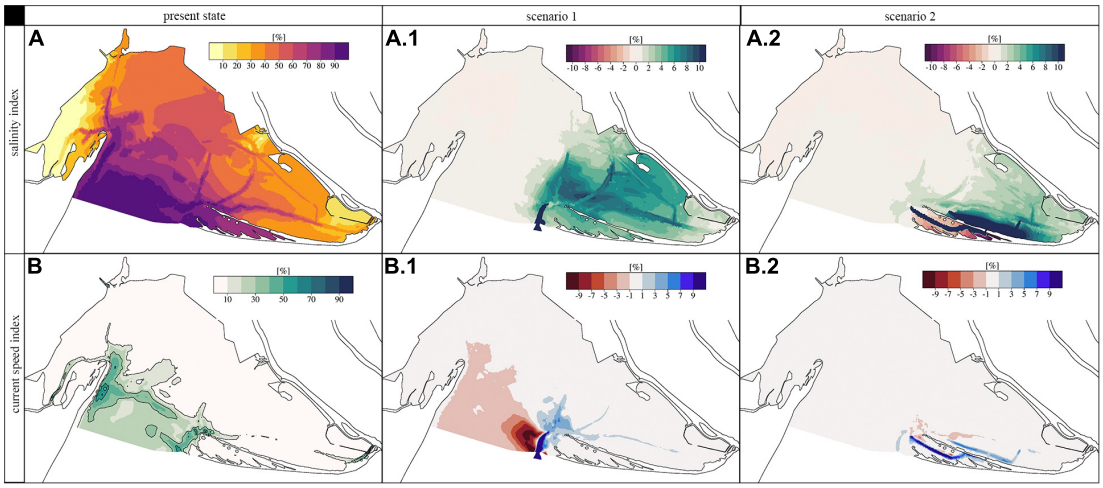

FIGURE 12 | Fitness indices of optimal growing conditions of the present state for salinity (FT2) and current speed (FT1). **(A)** FT2 present day; **(A.1)** difference between FT2 in the present day and Sc1 conditions; **(A.2)** difference between FT2 in the present day and Sc2 conditions. **(B)** FT1 present day; **(B.1)** difference between FT1 in the present day and Sc1 conditions; **(B.2)** difference between FT1 in the present day and Sc2 conditions.

ecosystem modeling, "What if" scenarios could be designed to answer additional management questions.

Local stakeholders wanted to know whether morphological interventions would have a positive impact on clam farming, and thus two morphology scenarios were investigated. The first scenario (Sc1) consisted in deepening and widening the eastern inlet channel (**Figure 1a**, red contour), which, as shown in the previous section, shows an important estuarine exchange with the open sea, with salt water entering at depth. Currently the eastern mouth has a width of about 50 m and a depth varying between a maximum of −5 m and a minimum of −1.5 m near the sea outlet, due to the littoral sand transport that is deposited in front of the inlet. The community of stakeholders asked what the hydrodynamics changes would be if the eastern mouth was enlarged to about 100 m, deepened up to 4 m everywhere and extended toward the sea (**Figure 1a**).

The second scenario (Sc2) consisted in dredging a channel that would extend from the eastern inlet channel to the easternmost side of the lagoon, crossing the area between the two spits of the Scanno of Goro, as shown by the orange line in **Figure 1a**. The stakeholders were interested to see whether the current and salinity conditions could be changed so that a clam nursery could be re-established between the spits. The stakeholders requested that the canal should have a width of 30 m and a depth of 3 m.

Numerical experiments were then carried out using these modifications in the model bottom bathymetry. The simulations were run for 2018 using the same atmospheric and river forcing as the present-day bathymetry conditions.

Differences between the present-day conditions and the scenarios were larger in Sc1 than Sc2 and in general were significant with respect to the mean current amplitudes in **Figure 4** (current changes are of the order of 1–5 cm s^{-1}). Differences were larger close to the specific bathymetry changes but some effects are evident, in the case of Sc1, in an area intercepted by a radius of about 2 km around the secondary mouth. Despite this, the increase in the tidal currents in the western channel is significant (8–10%) only in the peak values during the spring tide. The same analysis of the vertical structure of the flow carried out in **Table 3** shows that there were no significant changes: the inflow increased slightly in the third level at the expense of the flow in the middle layers. The net flux of the eastern channel did not change appreciably (-9 m^3 s^{-1}).

These differences however, were not sufficiently insightful to understand whether the morphological changes would be worth the effort. It was then decided to use two "fitness (FT) indices" developed in a previous study (Istituto Delta Ecologia Applicata, 2004). The FTs considered here are threshold values for the current intensity and water salinity, which vary between 0 and 1 for sub-optimal to optimal clam farming conditions. We considered only FTs ranging from 0.5 to 1, for the barotropic current speed and the bottom salinity. The corresponding optimal values for current amplitudes (FT1) are between 20 and 150 cm s^{-1}, and between 20 and 35 PSU for salinity (FT2). We then calculated the percentage of days in 2018 when FT1 and FT2 were above these optimal threshold values. The values of the FTs are shown in the **Supplementary Figure 4**.

Figure 12 shows the results for FT1 and FT2 in present day conditions and the difference between Sc1 and Sc2. The results confirm that today most of the farming areas are located where FT2 is higher than 60%. In contrast, FT1 seems to be a strong limiting factor for clam farming. This is partially true because normally the current speed is reduced to zero at each tidal inversion, and this lowers the percentage of days where the optimal FT1 values are achieved. In fact, the ex-nursery area is not favorable because of the very weak hydrodynamics, in agreement with the largest WRT values described before. Moreover, the areas of high riverine footprint are not suitable for clam farming, and the gates should be maneuvered carefully to ensure an acceptable value of FT2 during the early growing season of the clams.

In Sc1, changes in FT1 and FT2 optimal conditions are of the order of 10–12% and in a quite extended area of the eastern lagoon. However, on the western side of the eastern mouth, there is a negative impact which needs to be considered. In Sc2, changes are more significant for FT2 (up to +15% changes) but only in an area close to the bathymetry changes and not as wide area as in Sc1. In Sc2 FT1 changes are negligible.

Using only FT1 and FT2 indices for the Goro Lagoon, the preliminary conclusion is that multiple interventions would be required, and that local dredging would simply not induce large enough changes to impact on the optimal functioning of the lagoon.

SUMMARY AND CONCLUSION

In this paper we studied the circulation of the Goro lagoon and its connectivity with the open sea and we carried out "what if" scenarios for the optimal functioning of the lagoon as a clam farming site.

The Goro lagoon was modeled for the first time with the appropriate connections to the open ocean waters. This has been realized by a cascading model strategy from the large-scale ocean circulation, at the Mediterranean scale (CMEMS analyses), to the Adriatic intermediate model (AdriaROMS) and to the Goro lagoon marine areas with unstructured grid modeling. This model cascading is necessary to add processes at different space and time scales where and when it is needed. GOLFEM has 10 m resolution inside the lagoon, required to resolve the channels, and high frequency winds, as well as resolved interfaces with both the riverine inputs and the open sea.

The Goro lagoon is found to be an estuarine dominated area where exchanges with the open sea occur along two relatively deep lateral channels (5–6 m deep) and one shallow central tidal flat plateau. Across the latter there is only outflow of lagoon waters while at the two side channels along the inlet section, the flow is on average baroclinic. Open sea, relatively salty waters are exchanged from the bottom of the channels to about 2–3 m from the surface and this is the only source of open sea water entering the lagoon on a yearly average.

The tidal flow in the lagoon is dominated by semidiurnal tidal components and it is an important high frequency component of the circulation. The exchanges at the inlet section channels can be barotropic and baroclinic at different phases of the tidal flow and there are also hours of the day where the net flow through the inlet section is minimum and some days it remains baroclinic for several hours. The lagoon WRTs are from few days to more than a week, signaling the importance of the deep water inflow from the channels for the exchange of oxygen with the open sea waters.

The lagoon-river channels exchanges were analyzed and the mean values of the discharges and their salinities were calculated: the average river-channel volume flux enters the lagoon trough the Gorino lock and the Manufatto and the water is brackish because of the seawater intrusions in the Po of Goro branch. The salinity intrusion exceeded 20 km in August 2018 with the lowest discharge from the Po. Considering that the climate change scenarios project decreasing Po river discharges due to atmospheric drought conditions, the amplitude of the salt wedge is clearly a severe threat to the lagoon.

The results of this work are reliable and derive not only from the high resolution of the model, but also from the detailed knowledge of the lateral boundary conditions. Nevertheless, there is still uncertainties. Since the fast-evolving morphology is an important constraint on the lagoon dynamics, continuously updated, synoptic bathymetric surveys are fundamental, rather than multiple patch-like surveys. In addition to the natural variability of the hydrological forcing, the untracked opening/closing of the Gorino lock and Manufatto operated by the local authorities, are another source of uncertainty in simulating the circulation of the lagoon.

The changes in the circulation due to man-induced changes in bathymetry happen very rapidly due to the shallowness of the Lagoon and its fast WRTs. The assessment of the long period effects of bathymetric changes on the circulation implies morphological modeling and sediment transport, with all the assumptions regarding the sediment load boundary conditions from the river branches. This will be part of future investigations that are prepared by the present work in terms of a solid hydrodynamic modeling, coherent with the present data.

Goro Lagoon Finite Element Model was also conceived as a scientific tool to support decision makers in evaluating interventions for improving clam farming and the sustainable exploitation of the Goro lagoon. The high-resolution triangular grid can be easily adapted to represent the features of new channels that need dredging or deepening.

The "What if" scenarios described in this paper show that realistic and complex validated/calibrated hydrodynamic numerical models can help to reduce uncertainties regarding the impacts of different interventions. The difference with previous studies is that now the uncertainty related to the reproduction of the present day environmental marine conditions has been lowered to an acceptable value. The "What if" scenarios examined in this paper highlight that dredging might not always imply a change in hydrodynamic conditions leading to a significant change in fitness indices. The local dredging of canals inside the Scanno of Goro is clearly not sufficient to increase the current intensity and the salinity values to more suitable conditions for the clam farming of the lagoon.

Finally, this study demonstrates the importance of designing a seamless chain of models that integrate local effects into the initial fields derived from coarser operational models. Furthermore it poses already questions on the essential monitoring aspects of the lagoon which should consider bathymetric frequent surveys and a strict management of the man-made channel inflows. We believe that our findings demonstrate that the proper cascading approach can be a valid modeling methodology to face the challenges of predicting the Global Coastal Ocean in the next decade.

DATA AVAILABILITY STATEMENT

A public repository named "Downscaling of an unstructured model from the coastal-ocean to the Goro lagoon and the Po

river delta branches (Italy): results of the GOLFEM finite element model" was created and is accessible at 10.5281/zenodo.4072016.

The dataset comprehends the model outputs and the postprocessed results, converted in regular grid format (Netcdf) at 100 m and 50 m resolution, respectively, the time series of the freshwater discharges calculated on the basis of the raw data of the pumping stations, and the climatological time series of the water temperature for the Po river and the pumping stations.

AUTHOR CONTRIBUTIONS

NP, FM, and GU the study was designed (conceptualization and methodology). ST and SL were responsible for the field campaign and the collection of the data, that were analyzed by JA and FM. JA and FM performed the model setup, validation, and simulations. FM, NP, and JA conducted the analysis and discussion of the model results. FM wrote the Abstract, sections "Introduction," "Observations," "Results," and "The Golfem Model for the 'What If' Scenarios". JA wrote the section "The Numerical Model of the Goro Lagoon (GOLFEM)," and "Appendixes", reviewed by GV. NP wrote the section "Understanding the Lagoon Circulation." AV wrote the section "The Downscaling Approach." AV and TP were responsible for the project and the study as well as, together with SL, for the fundraising and the collaboration among CNR, UNIBO, and Arpae, and with the local stakeholders of the Goro Lagoon. All authors contributed to the article and approved the submitted version.

FUNDING

The GOLFEM model was realized thanks to the funds granted by the Emilia-Romagna law "L.R. 36/1995 e s.m.i. – Piano Operativo 2016–2017 – Anno 2017" and transferred to Arpae as decided by the "Comitato Operativo Sacca di Goro" in September 2017. Arpae, in turn, involved the Department of Physics and Astronomy of the University of Bologna and the Institute of Marine Sciences (Venice) of the National Research Council for the development of the model.

ACKNOWLEDGMENTS

We would like to thank the local stakeholders that helped to focus the work on important socio-economic activities, the improvement of the ecological value and the correct exploitation of the Goro Lagoon. We cite the Major of Goro, the technical office of the Goro Munipality, the local fisherman's consortium CO.Sa.Go., the Istituto Delta Ecologia Applicata for the valuable support, field information's transfer and the results discussions. Furthermore, we would also like to thank Dr. Paola Magri of the Arpae (local office of Ferrara) for the helpful interaction with the local stakeholders, the personnel of the Struttura Oceanografica Daphne – Unità Sacca di Goro, for the field campaign and information. We would also like to thank Eng. Laura Montanari from Consorzio di Bonifica Pianura di Ferrara for supplying the useful information about the drainage basin of the Goro Lagoon and the important data of the pumping stations. The GOLFEM simulations were mostly run on the Galileo supercomputer at the SCAI facility of CINECA in Bologna, freely available for the Ph.D. students at the University of Bologna, and on the Arpae-SIMC supercomputing facility.

SUPPLEMENTARY MATERIAL

The Supplementary Material for this article can be found online at: https://www.frontiersin.org/articles/10.3389/fmars.2021.647781/full#supplementary-material

REFERENCES

Aleynik, D., Dale, A. C., Porter, M., and Davidson, K. (2016). A high resolution hydrodynamic model system suitable for novel harmful algal bloom modelling in areas of complex coastline and topography. *Harmful Algae* 53, 102–117. doi: 10.1016/j.hal.2015.11.012

Alfieri, L., Salamon, P., Pappenberger, F., Wetterhall, F., and Thielen, J. (2012). Operational early warning systems for water-related hazards in Europe. *Environ. Sci. Policy* 21, 35–49. doi: 10.1016/j.envsci.2012.01.008

Aluie, H., Hecht, M., and Vallis, G. K. (2018). Mapping the energy cascade in the north atlantic ocean: the coarse-graining approach. *J. Phys. Oceanogr.* 48, 225–244. doi: 10.1175/JPO-D-17-0100.1

ARPA Veneto (2012). Agenzia Regionale per la Prevenzione e Protezione Ambientale del Veneto, Dipartimento Regionale per la Sicurezza del Territorio. Sulla Ripartizione Delle Portate del Po tra i vari Rami e le Bocche a Mare del Delta: Esperienze Storiche e Nuove Indagini All'anno 2011. Relazione 02/2012. Vicenza: ARPA Veneto.

Arpae (2018). *Agenzia Regionale per la Prevenzione, l'Ambiente e l'Energia dell'Emilia Romagna, Struttura Idro-Meteo-Clima, Servizio Idrografia e Idrologia Regionale e Distretto Po. Annali Idrologici 2018, Parte Seconda*. Bologna: Arpae.

Aubrey, D. G., and Friedrichs, C. T. (1996). *Buoyancy Effects on Coastal and Estuarine Dynamics*. Washington, DC: American Geophysical Union. doi: 10.1029/CE053

Bellafiore, D., Ferrarin, C., Braga, F., Zaggia, L., Maicu, F., Lorenzetti, G., et al. (2019). Coastal mixing in multiple-mouth deltas: a case study in the Po delta, Italy. *Estuar. Coast. Shelf Sci.* 226:106254. doi: 10.1016/j.ecss.2019.106254

Bellafiore, D., Ferrarin, C., Maicu, F., Manfè, G., Lorenzetti, G., Umgiesser, G., et al. (2021). Saltwater intrusion in a Mediterranean delta under a changing climate. *J. Geophys. Rese. Oceans* 126:e2020JC016437. doi: 10.1029/2020JC016437

Bezzi, A., Casagrande, G., Martinucci, D., Pillon, S., Del Grande, C., and Fontolan, G. (2019). Modern sedimentary facies in a progradational barrier-spit system: goro lagoon, Po delta, Italy. *Estuar. Coast. Shelf Sci.* 227:106323. doi: 10.1016/j.ecss.2019.106323

Blumberg, A. F., and Mellor, G. L. (1987). "A description of a three-dimensional coastal ocean circulation model," in *Coastal and Estuarine Sciences, Book 4,* ed. N. S. Heaps (Washington, DC: American Geophysical Union), 1–6.

Burchard, H. (2020). A universal law of estuarine mixing. *J. Phys. Oceanogr.* 2 81–93. doi: 10.1175/JPO-D-19-0014.1

Burchard, H., Bolding, K., and Villarreal, M. (1999). *GOTM-A General Ocean Turbulence Model.* Theory, Applications and Test Cases. European Commission Report EUR. Luxembourg: European Commission.

Carafa, R., Marinov, D., Dueri, S., Wollgast, J., Ligthart, J., Canuti, E., et al. (2006). A 3D hydrodynamic fate and transport model for herbicides in Sacca

di Goro coastal lagoon (Northern Adriatic). *Mar. Pollut. Bull.* 52, 1231–1248. doi: 10.1016/j.marpolbul.2006.02.025

Chiggiato, J., and Paolo, O. (2008). Operational ocean models in the Adriatic Sea: a skill assessment. *Ocean Sci.* 4:2008. doi: 10.5194/os-4-61-2008

Clementi, E., Oddo, P., Drudi, M., Pinardi, N., Korres, G., and Grandi, A. (2017). Coupling hydrodynamic and wave models: first step and sensitivity experiments in the Mediterranean Sea. *Ocean Dynamics* 67, 1293–1312. doi: 10.1007/s10236-017-1087-7

Coles, V. J., Brooks, M. T., Hopkins, J., Stukel, M. R., Yager, P. L., and Hood, R. R. (2013). The pathways and properties of the Amazon River Plume in the tropical North Atlantic Ocean. *J. Geophys. Res. Oceans* 118, 6894–6913. doi: 10.1002/2013JC008981

Correggiari, A., Cattaneo, A., and Trincardi, F. (2005). The modern Po Delta system: lobe switching and asymmetric prodelta growth. *Mar. Geol.* 222–223, 49–74. doi: 10.1016/j.margeo.2005.06.039

COSMO Newsletter (2004). Operational applications – ARPA-SIM (BOLOGNA). *Deutsch. WetterDienst (DWD) Offenbach* 6, 25–26.

Cucco, A., and Umgiesser, G. (2006). Modeling the venice lagoon residence time. *Ecol. Model.* 193, 34–51. doi: 10.1016/j.ecolmodel.2005.07.043

Doodson, A. T. (1928). *The Analysis of Tidal Observations: Series A, Containing Papers of a Mathematical or Physical Character227223–279*. London: Philosophical Transactions of the Royal Society. doi: 10.1098/rsta.1928.0006

Egbert, G. D., and Erofeeva, S. Y. (2002). Efficient inverse modeling of barotropic ocean tides. *J. Atmosph. Oceanic Technol.* 19, 183–204. doi: 10.1175/1520-04262002019<0183:EIMOBO<2.0.CO;2

Falcieri, M. F., Benettazzo, A., Sclavo, M., Russo, A., and Carniel, S. (2013). Po river plume pattern variability investigated from model data. *Contin. Shelf Res.* 87, 84–95. doi: 10.1016/j.csr.2013.11.001

Federico, I., Pinardi, N., Coppini, G., Oddo, P., Lecci, R., and Mossa, M. (2017). Coastal ocean forecasting with an unstructured grid model in the southern Adriatic and northern Ionian seas. *Nat. Hazards Earth Syst. Sci.* 17, 45–59. doi: 10.5194/nhess-17-45-2017

Ferrarin, C., Davolio, S., Bellafiore, D., Ghezzo, M., Maicu, F., Mc Kiver, W., et al. (2019). Cross-scale operational oceanography in the Adriatic Sea. *J. Operat. Oceanogr.* 12, 86–103. doi: 10.1080/1755876X.2019.1576275

Fofonoff, N. P., and Millard, R. C. Jr. (1983). *Algorithms for the Computation of Fundamental Properties of Seawater*. UNESCO Technical Papers in Marine Sciences, Vol. 44. Available online at: http://hdl.handle.net/11329/109

Fortunato, A., Oliveira, A., Rogeiro, J., Tavares da Costa, R., Gomes, J. L., Li, K., et al. (2017). Operational forecast framework applied to extreme sea levels at regional and local scales. *J. Operat. Oceanogr.* 10, 1–15. doi: 10.1080/1755876X.2016.1255471

Guarnieri, A., Pinardi, N., Oddo, P., Bortoluzzi, G., and Ravaioli, M. (2013). Impact of tides in a baroclinic circulation model of the Adriatic Sea. *J. Geophys. Res. Oceans* 118, 166–183. doi: 10.1029/2012JC007921

Harley, M. D., Valentini, A., Armaroli, C., Perini, L., Calabrese, L., and Ciavola, P. (2016). Can an early-warning system help minimize the impacts of coastal storms? A case study of the 2012 Halloween storm, northern Italy. *Nat. Hazards Earth Syst. Sci.* 16, 209–222. doi: 10.5194/nhess-16-209-2016

Hellerman, S., and Rosenstein, M. (1983). Normal monthly wind stress over the world ocean with error estimates. *J. Phys. Oceanogr.* 13, 1093–1104. doi: 10.1175/1520-04851983013<1093:NMWSOT<2.0.CO;2

Huang, B., and Mehta, V. M. (2010). Influences of freshwater from major rivers on global ocean circulation and temperatures in the MIT ocean general circulation model. *Adv. Atmos. Sci.* 27, 455–468. doi: 10.1007/s00376-009-9022-6

IPCC (2013). *Climate Change 2013: The Physical Science Basis. Contribution of Working Group I to the Fifth Assessment Report of the Intergovernmental Panel on Climate Change*. Cambridge: Cambridge University Press.

Istituto Delta Ecologia Applicata (2004). *Relazione Finale-Studio delle Potenzialità Produttive della Sacca di Goro*. Ferrara: Istituto Delta Ecologia Applicata.

Jeffries, M. A., and Lee, C. M. (2007). A climatology of the northern Adriatic Sea's response to bora and river forcing. *J. Geophys. Res. Oceans.* 112:C03S02. doi: 10.1029/2006JC003664

Jerlov, N. G. (1976). *Marine Optics*. Copenhagen: Elsevier oceanography series.

Kjerfve, B., and Magill, K. E. (1989). Geographic and hydrodynamic characteristics of shallow coastal lagoons. *Mar. Geol.* 88, 187–199. doi: 10.1016/0025-3227(89)90097-2

Kolmogorov, A. N. (1941). Equations of turbulent motion on an incompressible fluid, I Dokl. *Akad. Nauk SSSR* 30, 299–303, (English Translation: Imperial College, Mech. Eng. Dept. Rept. ON/6, 1968).

Ludwig, W., Dumont, E., Meybeck, M., and Heussner, S. (2009). River discharges of water and nutrients to the Mediterranean and Black Sea: major drivers for ecosystem changes during past and future decades? *Progr. Oceanogr.* 80, 199–217. doi: 10.1016/j.pocean.2009.02.001

Maicu, F., De Pascalis, F., and Ferrarin, C. (2018). Hydrodynamics of the po river-delta-sea system. *J. Geophys. Res. Oceans.* 123:3601. doi: 10.1029/2017JC013601

Marinov, D., Norro, A., and Zaldivar, J.-M. (2006). Application of COHERENS model for hydrodynamic investigation of Sacca di Goro coastal lagoon (Italian Adriatic Sea shore). *Ecol. Model.* 193, 52–68. doi: 10.1016/j.ecolmodel.2005.07.042

Marinov, D., Zaldivar, J. M., Norro, A., Giordani, G., and Viaroli, P. (2008). Integrated modelling in coastal lagoons: Sacca di Goro case study. *Hydrobiologia* 611, 147–165. doi: 10.1007/s10750-008-9451-8

O'Kane, J. P., Suppo, M., Todini, E., and Turner, J. (1992). Physical intervention in the lagoon of Sacca di Goro. An examination using a 3-D numerical model. *Mar. Coast. Eutrophic.* 126, 489–510. doi: 10.1016/B978-0-444-89990-3.50046-8

Orlić, M., Kuzmić, M., and Pasarić, Z. (1994). Response of the Adriatic Sea to the bora and sirocco forcing. *Contin. Shelf Res.* 14, 91–116. doi: 10.1016/0278-4343(94)90007-8

Paulson, C. A., and Simpson, J. J. (1977). Irradiance measurements in the upper ocean. *J. Physical Oceanography* 7, 952–956. doi: 10.1175/1520-04851977007<0952:IMITUO<2.0.CO;2

Pawlowicz, R., Beardsley, B., and Lentz, S. (2002). Classical tidal harmonic analysis including error estimates in MATLAB using T_TIDE. *Comput. Geosci.* 28, 929–937. doi: 10.1016/S0098-3004(02)00013-4

Pettenuzzo, D., Large, W. G., and Pinardi, N. (2010). On the corrections of ERA-40 surface flux products consistent with the Mediterranean heat and water budgets and the connection between basin surface total heat flux and NAO. *J. Geophys. Res. Oceans* 115:6022P. doi: 10.1029/2009JC005631

Prandtl, L., and Wieghardt, K. (1945). Über ein neues Formelsystem f ur die ausgebildete Turbulenz. *Nachr. Akad. Wiss. Göttingen Math. Phys. Kl.* 1, 6–19. doi: 10.1007/978-3-662-11836-8_72

Reed, R. K. (1977). On estimating insolation over the Ocean. *Phys. Oceanogr.* 7, 482–485. doi: 10.1175/1520-0485(1977)007<0482:OEIOTO>2.0.CO;2

Russo, A., Coluccelli, A., Carniel, S., Benetazzo, A., Valentini, A., Paccagnella, T., et al. (2013). *Operational Models Hierarchy for Short Term Marine Predictions: The Adriatic Sea Example. MTS/IEEE OCEANS – Bergen*. Bergen: IEEE, 1–6. doi: 10.1109/OCEANS-Bergen.2013.6608139

Sánchez-Arcilla, A., García-León, M., Gracia, V., Devoy, R., Stanica, A., and Gault, J. (2016). Managing coastal environments under climate change: pathways to adaptation. *Sci. Total Environ.* 572, 1336–1352. doi: 10.1016/j.scitotenv.2016.01.124

Simeoni, U., Fontolan, G., Tessari, U., and Corbau, C. (2007). Domains of spit evolution in the Goro area, Po Delta, Italy. *Geomorphology* 86, 332–348. doi: 10.1016/j.geomorph.2006.09.006

Smagorinsky, J. (1963). General circulation experiments with the primitive equation i the basic experiment. *Month. Weather Rev.* 91, 99–164. doi: 10.1175/1520-0493(1963)091<0099:GCEWTP>2.3.CO;2

Steppeler, J., Doms, G., Schättler, U., Bitzer, H. W., Gassmann, A., Damrath, U., et al. (2003). Meso-gamma scale forecasts using the nonhydrostatic model LM. *Meteorog Atmos Phys.* 82, 75–96. doi: 10.1007/s00703-001-0592-9

Syvitski, J. P. M., Kettner, A. J., Correggiari, A., and Nelson, B. W. (2005). Distributary channels and their impact on sediment dispersal. *Mar. Geol.* 222, 75–94. doi: 10.1016/j.margeo.2005.06.030

Tesi, T., Miserocchi, T., Goni, M. A., Turchetto, M., Langone, L., De Lazzari, A., et al. (2011). Influence of distributary channels on sediment and organic matter supply in event-dominated coastal margins: the Po prodelta as a study case. *Biogeosciences* 8, 365–385. doi: 10.5194/bg-8-365-2011

Tosi, L., Da Lio, C., Strozzi, T., and Teatini, P. (2016). Combining L- and X-Band SAR interferometry to assess ground displacements in heterogeneous coastal environments: the Po river delta and Venice lagoon, Italy. *Remote Sens.* 8:308. doi: 10.3390/rs8040308

Trotta, F., Pinardi, N., Fenu, E., Grandi, A., and Lyubartsev, V. (2017). Multi-nest high-resolution model of submesoscale circulation features in the Gulf of Taranto. *Ocean Dynam.* 67, 1609–1625. doi: 10.1007/s10236-017-1110-z

Umgiesser, G., Melaku Canu, D., Cucco, A., and Solidoro, C. (2004). A finite element model for the Venice Lagoon, development, set up, calibration and validation. *J. Mar. Syst.* 51, 123–145. doi: 10.1016/j.jmarsys.2004.05.009

Ursella, L., Poulain, P. M., and Signell, R. P. (2006). Surface drifter derived circulation in the northern and middle Adriatic Sea: response to wind regime and season. *J. Geophys. Res. Oceans* 112:C03S04. doi: 10.1029/2005JC003177

Valentini, A., Delli Passeri, L., Paccagnella, T., Patruno, P., Marsigli, C., Cesari, D., et al. (2007). The sea state forecast system of ARPA-SIM. *Boll. Geofis. Teor. Appl.* 48, 333–349.

Valle-Levinson, A., Huguenard, K., Ross, L., Branyon, J., MacMahan, J., and Reniers, A. (2015). Tidal and nontidal exchange at a subtropical inlet: destin Inlet, Northwest Florida. *Estuar. Coast. Shelf Sci.* 155:137. doi: 10.1016/j.ecss.2015.01.020

Valle-Levinson, A. (2010). "Definition and classification of estuaries," in *Contemporary Issues in Estuarine Physics*, ed. A. Valle-Levinson (Cambridge: Cambridge University Press), 1–11. doi: 10.1017/CBO9780511676567.002

Vallis, G. K. (2006). *Atmospheric and Oceanic Fluid Dynamics*. Cambridge: Cambridge University Press, 745.

Verri, G., Pinardi, N., Oddo, P., Ciliberti, S. A., and Coppini, G. (2018). River runoff influences on the Central Mediterranean overturning circulation. Clim. Dyn. 50, 1675–1703. doi: 10.1007/s00382-017-3715-9

Viaroli, P., Azzoni, R., Bartoli, M., Giordani, G., and Tajé, L. (2001). "Evolution of the Trophic conditions and dystrophic outbreaks in the sacca di goro lagoon (Northern Adriatic Sea)," in *Mediterranean Ecosystems*, eds F. M. Faranda, L. Guglielmo, and G. Spezie (Milano: Springer). doi: 10.1007/978-88-470-2105-1_5

Viaroli, P., Giordani, G., Bartoli, M., Naldi, M., Azzoni, R., Nizzoli, D., et al. (2006). "The Sacca di Goro and an arm of the Po river," in *Estuaries. The Handbook of Environmental Chemistry*, Vol. 5, ed. P. J. Wangersky (Berlin: Springer). doi: 10.1007/698_5_030

Williams, R. T. (1981). On the formulation of finite-element prediction models. *Month. Weather Rev.* 109, 463–466. doi: 10.1175/1520-04931981109<0463:OTFOFE<2.0.CO;2

Williams, R. T., and Zienkiewicz, O. C. (1981). Improved finite element forms for the shallow-water wave equations. *Int. J. Numer. Methods Fluids* 1, 81–97. doi: 10.1002/fld.1650010107

Zaldívar, J. M., Cattaneo, E., Plus, M., Murray, C. N., Giordani, G., and Viaroli, P. (2003). Long-term simulation of main biogeochemical events in a coastal lagoon: Sacca Di Goro (Northern Adriatic Coast, Italy). *Contin. Shelf Res.* 23, 1847–1875. doi: 10.1016/j.csr.2003.01.001

Conflict of Interest: The authors declare that the research was conducted in the absence of any commercial or financial relationships that could be construed as a potential conflict of interest.

APPENDIX A

Governing Equations

System of HYdrodynamics Finite Element Modules (SHYFEM) is a finite element 3D hydrodynamic model developed at ISMAR-CNR (Umgiesser et al., 2004). It is based on the solution of the primitive equations considering the hydrostatic and Boussinesq approximations. It runs on an unstructured grid with a staggered Arakawa B-grid type horizontal spacing. Scalar quantities are computed at nodes, while vectors are solved at the center of the element. The horizontal momentum equations integrated over a vertical layer are:

$$\frac{\partial U_l}{\partial t} + u_l\frac{\partial U_l}{\partial x} + v_l\frac{\partial U_l}{\partial y} + \int_{z_l}^{z_{l-1}} w\frac{\partial u}{\partial z}dz - fV_l = -gh_l\frac{\partial \zeta}{\partial x} - \frac{gh_l}{\rho_0}\int_{z_{l_{mid}}}^{0}\frac{\partial \rho'}{\partial x}dz - \frac{h_l}{\rho_0}\frac{\partial P_a}{\partial x} + \nabla_h\cdot(A_H\nabla_h U_l) + + \int_{z_l}^{z_{l-1}}\frac{\partial \tau_{xz}}{\partial z}dz \tag{A.1}$$

$$\frac{\partial V_l}{\partial t} + u_l\frac{\partial V_l}{\partial x} + v_l\frac{\partial V_l}{\partial y} + \int_{z_l}^{z_{l-1}} w\frac{\partial v}{\partial z}dz + fU_l = -gh_l\frac{\partial \zeta}{\partial y} - \frac{gh_l}{\rho_0}\int_{z_{l_{mid}}}^{0}\frac{\partial \rho'}{\partial y}dz - \frac{h_l}{\rho_0}\frac{\partial P_a}{\partial y} + \nabla_h\cdot(A_H\nabla_h V_l) + \int_{z_l}^{z_{l-1}}\frac{\partial \tau_{yz}}{\partial z}dz \tag{A.2}$$

where $\zeta = \zeta(x, y, t)$ is the free surface, $l = 1...N$ is the vertical layer index, starting with $l = 1$ for the surface layer and increasing with depth with $l = N$ being the bottom layer, $z_l = 0...N$ are the depths of the layer interfaces at the bottom with z_0 being the free surface ζ and z_N the bottom interface of the deepest layer, and $z_{l_{mid}}$ is the depth at the middle of layer l. u_l and v_l are horizontal velocity components, U_l and V_l are the horizontal velocities integrated over the layer l (layer transports) defined by $U_l = u_l h_l$ and $V_l = v_l h_l$. h_l is the layer thickness, P_a is the atmospheric pressure at the sea surface, g is the gravitational acceleration, ρ_0 is the reference density of sea water, $\rho = \rho_0 + \rho'$ is the water density with ρ' representing the perturbation of the density from the reference value ρ_0, A_H is the horizontal eddy viscosity ($m^2\ s^{-1}$) computed following the Smagorinsky formulation (Smagorinsky, 1963; Blumberg and Mellor, 1987), and w_l is the vertical velocity for layer l defined at the bottom interface. τ_{xz}, τ_{yz} are the turbulent shear stresses defined at the bottom interface of each layer and written according to the flux-gradient theory. Thus, the layer integral of the stress terms of Eqs A.1 and A.2 reads as follows:

$$\begin{aligned}\int_{z_l}^{z_{l-1}}\frac{\partial \tau_{xz}}{\partial z}dz &= \tau_{xz}^{z_{l-1}} - \tau_{xz}^{z_l} = Av\frac{\partial u_{l-1}}{\partial z} - Av\frac{\partial u_l}{\partial z}\\ \int_{z_l}^{z_{l-1}}\frac{\partial \tau_{yz}}{\partial z}dz &= \tau_{yz}^{z_{l-1}} - \tau_{yz}^{z_l} = Av\frac{\partial v_{l-1}}{\partial z} - Av\frac{\partial v_l}{\partial z}\end{aligned} \tag{A.3}$$

The turbulent shear stresses at the free surface, $\tau_{xz}^{z_0}$ and $\tau_{yz}^{z_0}$ are defined by the momentum surface boundary condition (Eq. A.16) while for the last layer, $l = N$, $\tau_{xz}^{z_N}$ and $\tau_{yz}^{z_N}$ are defined by the bottom boundary condition (Eq. A.17).

The continuity equation integrated over a vertical layer l is written as:

$$\frac{\partial U_l}{\partial x} + \frac{\partial V_l}{\partial y} = w_{z_l} - w_{z_{l-1}} \tag{A.4}$$

To note that at the top layer $l = 1$, the continuity equation has an additional term representing the time variability of the top layer thickness and thus it reads as reported below:

$$\frac{\partial h_1}{\partial t} + \frac{\partial U_1}{\partial x} + \frac{\partial V_1}{\partial y} = w_{z_1} - w_{z_0} \tag{A.5}$$

Integrating the continuity equation over the entire water column, the free surface equation can now be written as follows:

$$\frac{\partial \zeta}{\partial t} + \frac{\partial \hat{U}}{\partial x} + \frac{\partial \hat{V}}{\partial y} = P - E \tag{A.6}$$

where $\hat{U} = \sum U_i$ and $\hat{V} = \sum V_i$ are the components of the barotropic transport, E is the evaporation, and P is the precipitation. The boundary conditions of the Eqs (A.6) are (A.15).

The layer integrated salinity and temperature equations reads, respectively:

$$\frac{\partial\left(h_l S_l\right)}{\partial t} + U_l\frac{\partial S_l}{\partial x} + V_l\frac{\partial S_l}{\partial y} + \int_{z_l}^{z_{l-1}} w\frac{\partial S}{\partial z}dz = \nabla_h\cdot\left(K_H\nabla_h h_l S_l\right) + \int_{z_l}^{z_{l-1}}\frac{\partial}{\partial z}\left(K_V\frac{\partial S}{\partial z}\right)dz \tag{A.7}$$

$$\frac{\partial\left(h_l\theta_l\right)}{\partial t} + U_l\frac{\partial\theta_l}{\partial x} + V_l\frac{\partial\theta_l}{\partial y} + \int_{z_l}^{z_{l-1}} w\frac{\partial\theta}{\partial z}dz = \nabla_h\cdot\left(K_H\nabla_h h_l\theta_l\right) + \int_{z_l}^{z_{l-1}}\frac{\partial}{\partial z}\left(K_V\frac{\partial\theta}{\partial z}\right)dz + \frac{1}{\rho_0 C_p}\left(I(z_{l-1}) - I(z_l)\right) \tag{A.8}$$

where K_H and K_V are the horizontal and vertical turbulent diffusion coefficient respectively ($m^2\ s^{-1}$). S_l and θ_l are respectively the salinity and temperature in layer l. For both Eqs (A.7) and (A.8) the turbulent diffusive fluxes are written according to the flux-gradient theory, $\tau_{Sz} = K_V\frac{\partial S}{\partial z}$ and $\tau_{\theta z} = K_V\frac{\partial\theta}{\partial z}$, and their surface and bottom boundary conditions are defined in Eqs (A.19–A.21).

The last term in Eq. (A.8), containing $I(z)$, is the solar irradiance at depth z, parametrized with a double exponential according to Paulson and Simpson (1977), defined as:

$$\frac{I(z)}{Q_S} = Re^{-z/\xi_1} + (1-R)\,e^{-z/\xi_2} \tag{A.9}$$

Q_S is the irradiance at the sea surface (Wm^{-2}), ξ_1 and ξ_2 are the two length scales of penetration of the solar radiation in the visible spectrum, R is the percentage of entering radiation depending on the water type. In this work, Q_S is parametrized with the Reed's formula (Reed, 1977). Water is considered to be a type 9 Jerlov water (turbid water, Jerlov, 1976) with $\xi_1 = 0.325\ m$, $\xi_2 = 1.505\ m$ and $R = 0.72$.

The vertical momentum equation, layer integrated under the hydrostatic hypothesis, provides the hydrostatic pressure:

$$p_l\left(x, y, z_{l_{mid}}, t\right) = \rho_0 g\left(\xi - z_{l_{mid}}\right) + \int_{z_{l_{mid}}}^{0}\rho^{'g}dz \tag{A.10}$$

To complete the set of equations the density ρ is computed from salinity, temperature and pressure according to the UNESCO equation of state (Fofonoff and Millard, 1983):

$$\rho_l\left(x, y, z_{l_{mid}}, t\right) = \rho_l\left(S_l, \theta_l, p_l\right) \tag{A.11}$$

Turbulence Model

The vertical eddy viscosity, A_V, and diffusivity, K_V are computed trough the definition of a two-equation model using a k – ε scheme for the closure of the turbulence that is implemented in the GOTM model (Burchard et al., 1999) and is part of the SHYFEM code. The eddy viscosity and diffusivity are found applying the relation of Kolmogorov (1941) and Prandtl and Wieghardt (1945) which relates the turbulent coefficients to a velocity and a turbulent length scale:

$$A_V = c_\mu\sqrt{k}l + \nu_v, \qquad K_V = c_\mu^{'}\sqrt{k}l + \gamma_v \tag{A.12}$$

where k is the turbulent kinetic energy, l is a turbulent length scale, ν_V and γ_V are respectively the molecular viscosity and diffusivity while c_μ and $c_\mu^{'}$ are dimensionless stability functions. In order to find the value for the vertical turbulent coefficients, the GOTM model solves an equation for the turbulent kinetic energy, k and an equation for the turbulence dissipation, ε defined as:

$$\frac{\partial k}{\partial t} + \overrightarrow{U}\cdot\nabla k = \frac{\partial}{\partial z}\left(\frac{A_v}{\sigma_k}\frac{\partial k}{\partial z}\right) + P_s + B - \varepsilon \tag{A.13}$$

$$\frac{\partial\epsilon}{\partial t} + \overrightarrow{U}\cdot\nabla\epsilon = \frac{\partial}{\partial z}\left(\frac{A_v}{\sigma_\epsilon}\frac{\partial\epsilon}{\partial z}\right) + \frac{\epsilon}{k}\left(c_{\epsilon 1}P_s + c_{\epsilon 3}B - c_{\epsilon 2}\epsilon\right) \tag{A.14}$$

where σ_k and σ_ε are the turbulent Schmidt number respectively for k and ε, P_S is the turbulent production by shear, B is the buoyancy production/destruction term while $c_{\varepsilon 1}$, $c_{\varepsilon 2}$, and $c_{\varepsilon 3}$ are empirical constants. The classical energy cascade model lead to a relation between k, ε, and l expressed by the following:

$$l = \left(c_{\mu}^{0}\right)^{3} \frac{k^{3/2}}{\epsilon} \tag{A.15}$$

where c_{μ}^{0} is an empirical constant. Once Eqs (A.13) and (A.14) are numerically solved, we can retrieve the turbulence length scale from Eq. (A.15) and compute the vertical eddy viscosity and diffusivity from Eq. (A.12).

Boundary Conditions

The Surface and Bottom Boundary Conditions

The vertical velocity at the bottom and at the surface, w_B and w_0, respectively, are given by the kinematic conditions, which are:

$$w_0 = \frac{D\zeta}{Dt}|_{\zeta} + E - P; \; w_B = 0 \tag{A.16}$$

where E is the evaporation and P is the precipitation rate.

The river runoff is not included in the surface boundary condition because it enters the lateral open boundary condition at the coastline where are the river mouths (see sub-section "The Lateral Boundary Conditions").

The wind stress, applied at the air-sea interface, is treated following the MFS bulk formulae approach (Pettenuzzo et al., 2010):

$$\tau_{xz}^{z_0} = A_v \frac{\partial u}{\partial z}|_{\zeta} = \frac{\rho_a}{\rho_0} C_D \left|\overrightarrow{u}_w\right| u_w \qquad \tau_{yz}^{z_0} = A_v \frac{\partial v}{\partial z}|_{\zeta} = \frac{\rho_a}{\rho_0} C_D \left|\overrightarrow{u}_w\right| v_w \tag{A.17}$$

where ρ_a is the air density, u_w and v_w the wind velocity components at 10 m and C_D is the wind drag coefficient computed with the Hellerman and Rosenstein's (1983) formulation.

At the bottom (layer N), the turbulent momentum stresses are computed following a quadratic formulation as follows:

$$\tau_{xz}^{z_N} = A_v \frac{\partial u}{\partial z}|_{z_N} = \frac{C_B}{H_N^2} \left|\overrightarrow{U_N}\right| U_N \qquad \tau_{yz}^{z_N} = A_v \frac{\partial v}{\partial z}|_{z_N} = \frac{C_B}{H_N^2} \left|\overrightarrow{U_N}\right| V_N \tag{A.18}$$

where H_N is bottom layer thickness, U_N and V_N the zonal and meridional transports of the bottom layer. C_B is a bottom drag coefficient defined as:

$$C_B = \left(\frac{0.4}{ln\left(\frac{\lambda_B + 0.5H_N}{\lambda_B}\right)}\right)^2 \tag{A.19}$$

where λ_B is a bottom roughness length expressed in m, which varies spatially ranging from 0.005 in lagoon shallows to 0.08 in floodplains. These values were found during the calibration phase.

The air-sea interface temperature diffusive flux is:

$$\tau_{\theta z}^{z_0} = K_V \frac{\partial \theta}{\partial z}|_{\zeta} = \theta_{l=1} (E - P) - \frac{Q_{net}}{\rho_0 C_p} \tag{A.20}$$

where $Q_{net} = Q_S - Q_L - Q_H - Q_E$ is the net downward heat flux with Q_S the shortwave radiation flux, Q_L the longwave radiation flux, Q_E the latent heat flux and Q_H the sensible heat flux (Pettenuzzo et al., 2010). The C_P coefficient is the specific heat of the sea water.

The salt diffusive flux at the surface is:

$$\tau_{Sz}^{z_0} = K_V \frac{\partial S}{\partial z}|_{\zeta} = S_{l=1} (E - P) \tag{A.21}$$

The adiabatic bottom boundary conditions are applied for the tracers:

$$\tau_{\theta z}^{z_N} = K_V \frac{\partial \theta}{\partial z}|_{z_N} = 0 \qquad \tau_{Sz}^{z_N} = K_V \frac{\partial S}{\partial z}|_{z_N} = 0 \tag{A.22}$$

The Lateral Boundary Conditions

The rivers enter the lateral open boundary conditions along the coastline where the river mouths are located. The riverine release is provided in terms of prescribed runoff, temperature and salinity. The other lateral boundary along the coast is the closed land boundary where the velocity component normal to the boundary is set to zero and the tangential velocity follows the full-slip boundary condition.

At the offshore lateral open boundaries, the Dirichlet boundary condition is set for the sea surface height. The tracers follow the Dirichlet condition if the flux is entering the domain, otherwise a zero-gradient condition (Neumann boundary condition) is adopted. A nudging procedure is used for the horizontal velocities, with a nudging time of 30 min.

Spatial and Temporal Discretization

A semi-implicit time stepping of the divergence term of the free surface equation is used together with a semi-implicit formulation of the barotropic pressure gradient term and the Coriolis term of the momentum equation. The vertical mixing terms and the vertical advection of tracers are fully implicitly solved while the horizontal mixing terms, the horizontal advection of tracers and the horizontal and vertical advection of momentum are explicitly time stepped.

The domain is divided into triangular elements. The vertices of these elements are called nodes. The horizontal discretization uses staggered finite elements and is realized by expanding all the variables into form functions. The staggered finite elements approach ensures correct propagation of gravity waves and geostrophic adjustment, as shown in Williams (1981) and Williams and Zienkiewicz (1981). The staggered grid guarantees mass conservation and a feasible implementation of the semi-implicit time scheme.

The vertical discretization uses N layers where density, velocity components and tracers are supposed to be constant. The first layer has a variable thickness due to the variations in sea level, all the others have constant thickness in time. The last layer changes thickness according to the bathymetry (so-called partial step). The turbulent and molecular stresses and the vertical velocity are computed at the bottom interface of each layer, whereas all the other variables are defined at the layer center.

APPENDIX B

Statistical Indexes

Four statistical indexes are used to evaluate the model results during the phase of calibration and validation of the model. Correlation R, BIAS, root mean square error (RMSE) and the mean absolute error (MAE) are computed. In the following definitions we indicate the model output as ϕ_m^i while the observations are indicated as ϕ_o^i, where $i = 1, 2, 3. . .N$ is the number of observations.

The correlation index R indicates the linear relationship between two statistical variables and is defined as:

$$R = \frac{\frac{1}{N}\sum_{i=1}^{N}\left(\phi_m^i - \overline{\phi_m^i}\right)\left(\phi_o^i - \overline{\phi_o^i}\right)}{\phi_{\sigma m}\phi_{\sigma o}}$$

$\phi_{\sigma m}$ and $\phi_{\sigma o}$ are model output and observations standard deviation. The correlation index R ranges between -1 and 1. A value of 1 indicates a full linear relationship between the variables. Values around 0 indicates no correlation between the variables and a value of -1 indicates that the variables are inversely correlated.

The BIAS, RMSE and MAE are defined as follow:

$$\text{BIAS} = \frac{1}{N}\sum_{i=1}^{N}\left(\phi_m^i - \phi_o^i\right)$$

$$\text{RMSE} = \sqrt{\frac{1}{N}\sum_{i=1}^{N}\left(\phi_m^i - \phi_o^i\right)^2}$$

$$\text{MAE} = \frac{1}{N}\sum_{i=1}^{N}\left|\phi_m^i - \phi_o^i\right|$$

For each station where observations were collected, we choose the closest model node for ϕ_m^i.